AIMS Energy, 6 (4): 593–606.
DOI: 10.3934/energy.2018.4.593
Received: 15 July 2018
Accepted: 10 August 2018
Published: 17 August 2018

http://www.aimspress.com/journal/energy

Research article

Performance evaluation of polyaniline-based redox capacitors with respect to polymerization current density

W.A.D.S.S. Weerasinghe, K.P. Vidanapathirana* and K.S. Perera

Department of Electronics, Faculty of Applied Sciences, Wayamba University of Sri Lanka, Kuliyapitiya, 60200 Sri Lanka

*** Correspondence:** Email: kamalpv41965@gmail.com; Tel: 94-714411396.

Abstract: Supercapacitors (SCs) are promising alternative energy storage devices due to their relatively fast rate of energy storage and delivery. Redox capacitors in the family of SCs are based on conducting polymer (CP) or transition metal oxide electrodes. In this study, symmetric redox capacitors have been fabricated utilizing the CP, polyaniline (PANI) as electrodes and a gel polymer electrolyte (GPE) based on polyvinylidenefluoride (PVdF) as the electrolyte. Investigations have been carried out to study the effect of polymerization current density of PANI electrodes on the performance of redox capacitors. Polymerization current density was varied from 4 mA cm^{-2} to 9 mA cm^{-2} and the performance of redox capacitors was evaluated using electrochemical impedance spectroscopy (EIS), cyclic voltammetry (CV) test and galvanostatic charge discharge (GCD) test. EIS results showed that redox capacitor having electrodes prepared using the current density 7 mA cm^{-2} has the lowest charge transfer resistance and CV test elucidated that the same redox capacitor has maintained around 80% of maximum specific capacity from its initial value after 200 cycles. GCD results exhibited the highest specific discharge capacity of 421.4 F g^{-1}, specific power density of 935.6 W kg^{-1} and specific energy density of 8.0 Wh kg^{-1} after 200 cycles for the same capacitor.

Keywords: polyaniline; redox capacitor; gel polymer electrolyte; cyclic voltammetry; electrochemical impedance spectroscopy

1. Introduction

Supercapacitors (SCs) and batteries are the state-of-the-art electrical energy storage devices. SCs are preferable than batteries when high power density, fast charge-discharge rate and long life cycles are required [1]. Depending on the charge storage mechanism and type of electrodes, SCs can be classified into two categories as electric double layer capacitors (EDLCs) and redox capacitors. EDLCs are made up of carbon-based electrodes whereas redox capacitors are having electrodes based on conducting polymers (CPs) or transition metal oxides [2]. EDLC utilizes mainly the separation of the electronic and ionic charge at the interface between electrode materials and electrolyte solution. Although SCs are having high power density, still they were unable to produce the high energy density requirement especially for the application in electric vehicles. There is a new trend in developing hybrid SCs to find a solution to the low energy density of SCs [3,4]. Different materials such as carbon, oxide, and metal materials, are employed in the negative and positive electrode of hybrid SCs [5,6]. Redox capacitor provides its capacitance from faradic or pseudo redox reactions occurring within the active materials of electrode [7]. CPs usually grow in three–dimensional structures, introducing high porosity and roughness, which generate a large surface area favorable for enhancing electrochemical reactions [8]. They store and release charge through redox processes, resulting in so–called pseudo capacitance. Charging in a CP takes place throughout the bulk volume of the polymer, not just on the surface as is the case with the materials used for EDLCs. With this route the specific capacitance of a redox capacitor increases greatly. The fast charge-discharge processes associated with CPs give rise to high specific power too [9]. Polyaniline (PANI) is one of the most extensively used CPs for engineering redox capacitors [8–10]. PANI has multiple redox states (Leucoemeraldine, Emeraldine and Pernigraniline), high doping-dedoping rates during charging-dischargeing and good environmental stability [10]. Conditions used in the polymerization of PANI have very high contribution to the characteristics of the resulting polymer [8–11]. The surface structure of the electropolymerized film is affected by the conditions used for the electropolymerization such as current density, monomer concentration and types of solvent used [12]. Hence, the conductive property of the film is expected to change due to the morphological difference in the film [13]. In this study, the effect of polymerization current density on the performance of PANI electrodes in a redox capacitor was investigated.

2. Materials and methods

2.1. Preparation of electrodes

The monomer aniline (Aldrich) was distilled and stored under refrigeration prior to use. PANI films were galvanostatically electropolymerized on to commercial grade stainless steel (type 304) electrodes using a three-electrode set up where Ag/AgCl and Pt electrode were served as reference and counter electrodes respectively. The monomer concentration was 0.4 M and 0.5 M concentrated sulfuric acid (H_2SO_4–Aldrich) was used as the oxidizing agent. It has been reported that polymerization of aniline does not take place properly at low polymerization current densities [14]. In this study, polymerization current density was varied from 4 mA cm^{-2} to 9 mA cm^{-2} while maintaining a charge density of 1200 mC cm^{-2}. The area of deposition was 1 cm^2. After

polymerization, films were rinsed with distilled water and allowed to dry. The mass of the PANI film was 0.4 mg.

2.2. Preparation of gel polymer electrolyte (GPE)

Polyvinylidene fluoride (PVdF) (Aldrich), ethylene carbonate (EC) (98%, Aldrich), propylene carbonate (PC) (99%, Aldrich) and sodium thiocyanate (NaSCN) (99%, Aldrich) were used as received. EC and PC weight ratio was fixed as 1:1. Firstly,the required amount of PVdF was dissolved in an EC, PC mixture and magnetic stirring was done. Then, NaSCN was added to the mixture and stirring was continued. After that, the mixture was heated at 120 ^{o}C for 30 minutes. A very thin gel polymer electrolyte film was obtained from the hot press method and they were left overnight in a vacuum desiccator [15]. The composition of the GPE was 16PVDF/40EC/40PC/3NaSCN in weight basis [16].

2.3. Fabrication of redox capacitors

Sandwich-type symmetric redox capacitors were fabricated using two PANI electrodes. GPE having same the area of the electrode was served the electrolyte. Structure of the redox capacitor was in the form of PANI/PVdF:EC:PC:NaSCN/PANI. Several redox capacitors were fabricated using electrodes prepared with polymerization current densities from 4 to 9 mA cm^{-2}.

2.4. Characterization

2.4.1. Electrochemical impedance spectroscopy (EIS)

EIS measurements of redox capacitors were taken within the frequency range from 0.4 MHz to 0.01 Hz using a frequency response analyzer (Metrohm AUTOLAB 101). Impedance data were analyzed using non–linear least square fitting program [17]. By observing the electrochemical impedance plots or Nyquist plots, variation of the charge transfer resistance (R_{ct}) and bulk electrolyte resistance (R_b) with the polymerization current density of PANI electrode was determined. The high-frequency region plot and the mid frequency region of the Nyquist gives the value of R_b and R_{ct} respectively [18].

Specific capacitance (C_{SC}) of redox capacitors can be calculated using the Nyquist plot as well as the Bode plot (plot of the real part of capacitance (C') vs frequency). When using the Nyquist plot, C_{SC} was calculated using the equation,

$$C_s = 1/(2\pi f z'' m) \tag{1}$$

Here, f is the lowest frequency and Z" is the imaginary part of the impedance at frequency, f and m is the mass of a single electrode. Using the bode, single electrode capacitance C_{SC} was found at the maximum C'. Relaxation time (τ) was determined using the bode plot drawn between the imaginary part of capacitance (C'') vs frequency [19–21] using the equation,

$$\tau_0 = 1/(2\pi f_0) \tag{2}$$

where f_0 corresponds to the frequency at the maximum C''.

2.4.2. Cyclic voltammetry (CV) test

CV tests were performed for all the redox capacitors having PANI electrodes polymerized using different current densities in the potential window of 0.8 V–(−0.2) V at the scan rate of 5 m Vs^{-1} by means of a computer controlled potentiostat / galvanostat (Metrohm- AUTOLAB 101). One PANI electrode was served as the working electrode and the other as both the counter and the reference electrodes. Using cyclic voltammogram, single electrode (C_{sc}) specific capacity was calculated with the equation,

$$C_{SC} = 2\,I\,dv/(m\Delta vs) \tag{3}$$

Here, $\int I\mathrm{d}v$ is the integrated area of the cyclic voltammogram, m is the mass of single electrode, Δv is the potential window and s is the scan rate [19–21].

2.4.3. Galvanostatic charge–discharge (GCD) test

Charge-discharge test of redox capacitors was done in the potential limits of 0.0 V to 0.4 V for 200 cycles. The maximum charge and discharge currents were set to 1.25 mA. Using the charge-discharge curves, specific discharge capacity (C_d) of the redox capacitor was calculated using the equation,

$$C_d = \frac{I}{m\left(\frac{dv}{dt}\right)} \tag{4}$$

where, I is the constant discharge current, dt is the discharge time and dv is the potential drop upon discharging excluding IR drop.

Specific energy density (E_s) and specific power density (P_s) were calculated using equations

$$E_s = \frac{1}{2} C_d v^2 \tag{5}$$

$$\text{and } P_s = \frac{E_s}{t} \text{ [19–20]} \tag{6}$$

here, C_d is the specific discharge capacitance, v is the charging potential and t is the discharging time.

2.4.4. Morphological study

Scanning electron micrograph (SEM) images were obtained for PANI films prepared on FTO strips at different current densities.

3. Results and discussion

3.1. Polymerization

Changes in the polymerization potential with the time during electro polymerization of the PANI films with changing polymerization current densities are shown in the Figure 1.

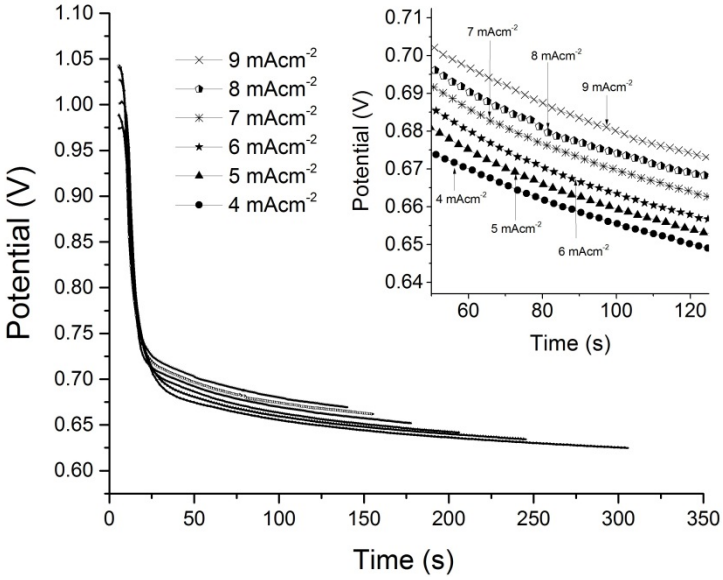

Figure 1. Chronopotentiograms of PANI films polymerized at different polymerization current densities of 4 to 9 mA cm^{-2}.

From Figure 1, it can be seen that the potential of nucleation, where the growth of PANI occurred, is varied with current density. Higher current densities have higher polymerization potentials while lower potentials mark the lower current densities. This may affect the surface structure and morphology of the film. According to Wang, et al., it is expected that roughness of the film increases with the polymerization current density [13]. Also the surface of the film deposited at high current densities seems to be like more "grainy" [13]. Due to this occurrence the electron movement becomes easier in the electrodes deposited at higher polymerization current densities [13].

3.2. Electrochemical impedance spectroscopy

For this type of a system impedance plot should consist of three main regions [22]. They are high frequency region, mid-frequency region and low-frequency region. The characteristics of the electrolyte are shown in the high frequency region by a semi-circle. Mid frequency region represents charge transfer resistance at the electrode/electrolyte interface and the Warburg diffusion. The capacitive properties become dominant at low frequencies and hence, low frequency region in the impedance plot illustrates the capacitive behavior with a spike. If the device shows a proper capacitive behavior, the corresponding spike is parallel to the imaginary axis of the impedance plot. In practical, this does not happen commonly due to several problems such as electrode surface roughness and irregularities of the electrodes. In the resulting impedance plot in Figure 2, the high

frequency semi-circle was not present. It may be due to the unavailability of required high-frequency region in the frequency response analyzer used. The steep rising response of impedance measurements in the very low frequency region is an indication for the capacitive behavior of PANI electrodes. The resulting line is not perfectly parallel to Z" as for a typical capacitive behavior. It may be due to the surface roughness as well as non-uniform active layer thickness [23].

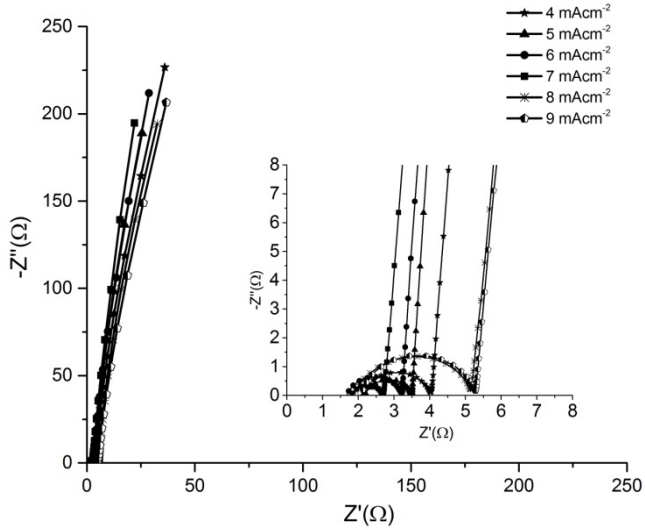

Figure 2. Nyquist plots within the frequency range 0.4 MHz to 0.01 Hz for the PANI/GPE/PANI redox capacitors fabricated using electrodes prepared with different polymerization current densities.

Table 1. Changes in the charge transfer resistance (R_{ct}) of PANI electrodes with the polymerization current density.

Current density/mA·cm^{-2}	R_{ct}/Ω
4	4.0
5	3.5
6	3.2
7	2.7
8	5.7
9	5.9

According to Figure 2 and table 1, it is clear that the R_{ct} has decreased with the increase of the current density up to 7 mA cm^{-2}. After that it has started to increase with the increment of the current density. This contradicts the conclusion of Wang, et al. [13]. According to them, films with higher current densities provide easy pathways to electrons to move. Based on the results obtained in this study, it can be mentioned that up to a certain current density electron movement follows the increase of current density as reported by Wang et al. [13]. However, there is a limiting current density for this behavior and beyond that it would fade.

Figure3 (a) and (b) are the resulting bode plots drawn between the real part of the capacitance

($C^{'}$) vs frequency and imaginary part of the capacitance ($C^{''}$) with frequency.

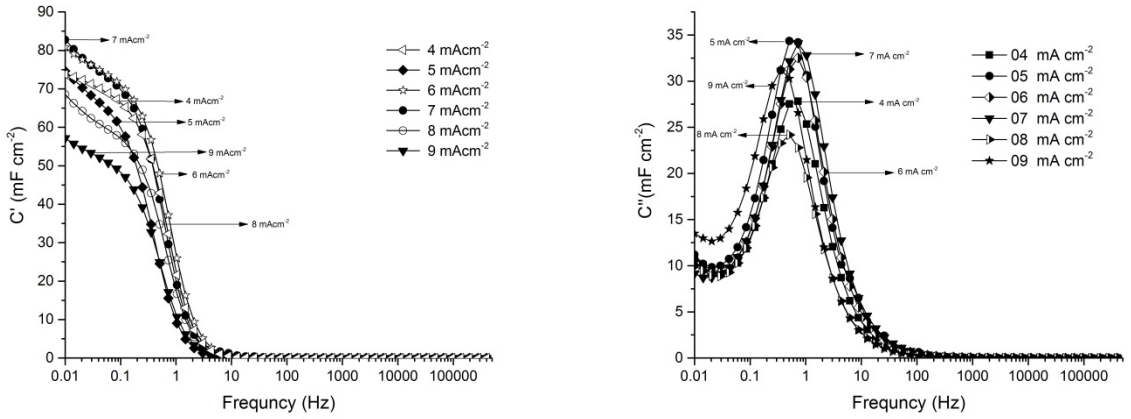

(a) (b)

Figure 3. (a) and (b) Resulting bode plots of redox capacitors with respect to different current densities used for polymerization of PANI electrodes.

Single electrode capacitance ($C^{'}_{SC}$) values and the calculated relaxation time (τ) with respect to different current densities are given in the table 2.

Table 2. Change in single electrode capacitance and relaxation time with the polymerization current density.

Current density/mA cm^{-2}	$C^{'}$/mF cm^{-2}	τ/s
4	73.8	0.308
5	74.6	0.292
6	80.7	0.218
7	82.7	0.193
8	68.5	0.312
9	57.1	0.447

Low values of τ suggest speedy redox reactions resulting quick ion transfer taking place between electrodes and electrolyte [24].

3.3. Cyclic voltammetry test

Cyclic voltammograms obtained for redox capacitors with PANI electrodes polymerized using different current densities and cycled in the potential window of −0.2 V to 0.8 V are shown in Figure 4.

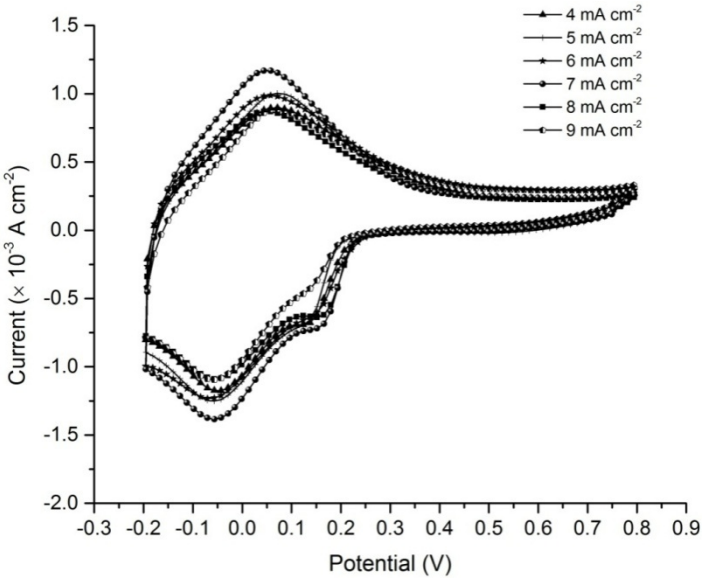

Figure 4. Cyclic voltammograms of PANI/GPE/PANI redox capacitors having PANI electrodes polymerized with different current densities. Scan rate 5 mV s^{-1}.

It shows peaks correspond to both the cathodic and anodic cycles as a result of redox processes that take place in the redox capacitor.

The electrode morphology has a considerable impact on the electrochemical behavior of PANI [6]. This is the reason that the shapes of the cyclic voltammograms for similar PANI electrodes reported in the literature are significantly different. While some exhibit three well-defined redox states [25,26], others show a single state [27,28].

Single electrode specific capacity variation over 200 continuous cycling of redox capacitors having PANI electrodes prepared with different polymerization current densities is given in table 3.

Table 3. Single electrode specific capacity (C_{sc}) of the redox capacitors with respect to polymerization current density of PANI electrodes calculated from the cyclic voltammograms.

Polymerization current density/mA cm^{-2}	C_{sc}/F g^{-1} First cycle	C_{sc}/F g^{-1} After 200 cycles
4	557.9	426.9
5	579.9	445.8
6	620.5	489.0
7	659.2	524.0
8	550.8	400.0
9	532.0	337.1

Results show that specific capacity increases up to a peak value with the increment of polymerization current density and starts to reduce with the further increase of the current density. This may be due to a change in the morphology of the PANI electrode after a certain value of the

polymerization current density which affects to the redox reactions that take place between PANI electrode and the GPE. This variation tallies with the results obtained with EIS. Degradation of the capacity was observed with the cycle number. This may be due to lack of full reversibility and less cycling efficiency as a result of side reactions. However, compared to others, redox capacitor with PANI electrodes of 7 mA cm^{-2} current density has maintained around 80% of specific capacity retention from its initial value after 200 cycles.

3.4. Galvanostatic charge-discharge test

Figure 5 shows the continuous charge discharge curves of 7 mA cm^{-2} current density PANI film based redox capacitor and it proves that good stability has been maintained over 200 cycles. Near linear and symmetric charge and discharge curves within the potential window of 0 V and 0.4 V suggest a good capacitive performance with a rapid I–V response [29]. Also, symmetric charge profile suggests a pseudocapacitive characteristic and good capacitive behavior of the electrodes [8].

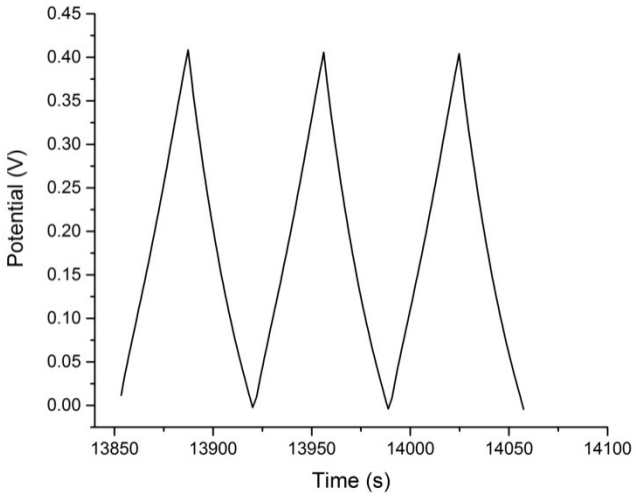

Figure 5. Galvanostatic charge-discharge curves of redox capacitor having PANI electrodes prepared with 7 mA cm^{-2} polymerization current density.

Energy efficiency of the redox capacitors with the change in the polymerization current density of PANI electrodes were calculated using the equation

$$\eta = E_d / E_c \text{ [30]} \tag{7}$$

where E_d is the discharged energy and E_c is charged energy.

Table 4 shows the comparison of the specific discharge capacity, specific energy density, specific power density, and energy efficiency after 200 continuous galvanostatic charge-discharge cycling of redox capacitors having PANI electrodes made with different polymerization current densities. Highest specific discharge capacity of 421.4 F g^{-1}, specific energy density of 8.0 Wh Kg^{-1} and specific power density of 935.6 W kg^{-1} values were recorded for 7 mA cm^{-2} current density

PANI films based redox capacitor. Maximum specific capacity value obtained in this study is higher than the reported values in the range of 80–250 F g^{-1} [10,31,32]. It was observed that when the current density was increased from 4 mA cm^{-2} to 7 mA cm^{-2}, energy efficiency increased by 18.8% and the maximum value of 85.0% was recorded by the capacitor with 7 mA cm^{-2} current density PANI films. With the further increase of current density up to 9 mA cm^{-2} energy efficiency was reduced by 24.8%.

Table 4. Comparison of specific discharge capacity (C_d), specific energy density (E_s), specific power density (P_s), and energy efficiency (ŋ) of redox capacitors with the variation of the polymerization current density of PANI electrodes.

Polymerization current density/mA cm^{-2}	C_d/F g^{-1}	E_s /Wh kg^{-1}	P_s/W kg^{-1}	ŋ%
4	306.0	4.4	699.1	66.2
5	324.4	5.5	775.1	70.0
6	358.8	6.5	840.5	76.3
7	**421.4**	**8.0**	**935.6**	**85.0**
8	281.0	4.0	610.2	63.4
9	270.4	559.3	3.2	60.2

3.5. Morphological studies

Figure 6 shows the SEM images of PANI films fabricated with the polymerization current densities of 4, 7 and 9 mA cm^{-2}.

It can be seen that all samples are having porous structures. Fig 6 (a) and (b) are composed of nanofibers. With the polymerization current density, the quantity of these nanofibers increases, whereas their diameter decreases. This may be due to the fact that aniline is easier to be oxidized into radical cations at higher potential caused by larger current density, resulting in more nuclei, supporting the grow of nanofibers during the next polymerization [33]. Further increase of current density to 9 mA cm^{-2} resulted a film with less porous flake type morphology Figure 6 (c)

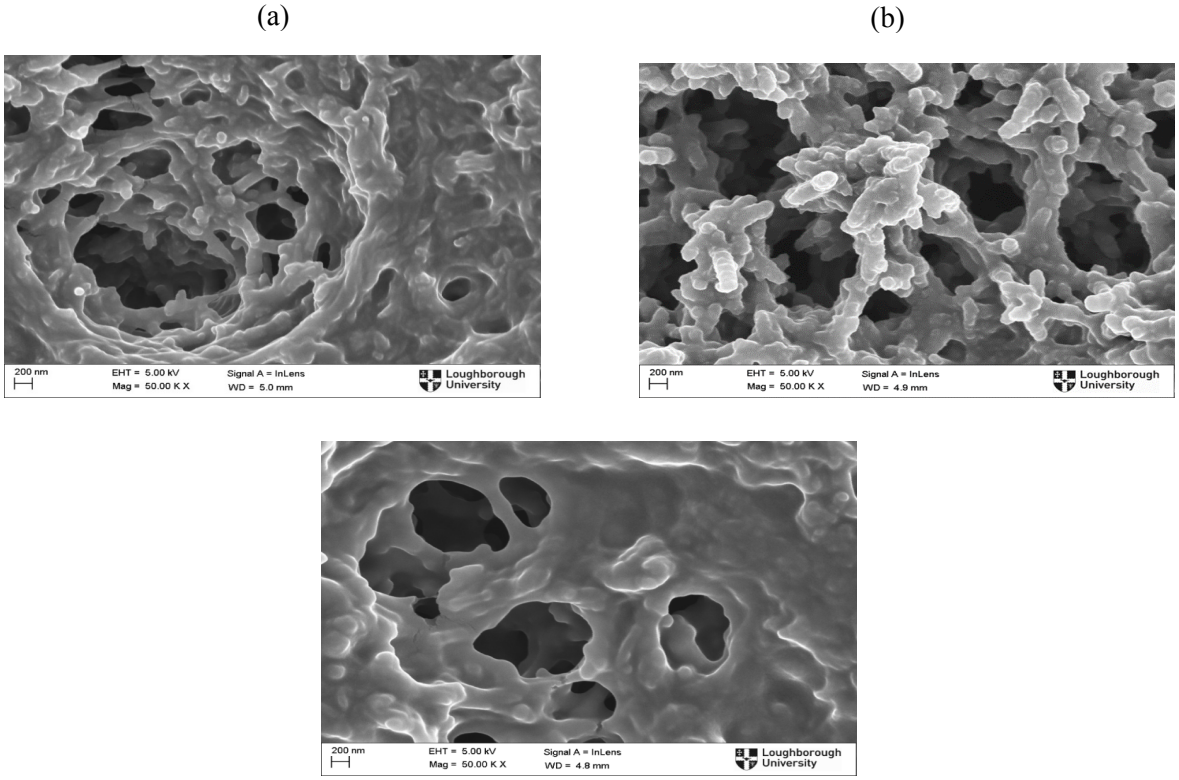

Figure 6. SEM images of PANI films synthesized at different polymerization current densities: (a) 4 mA cm^{-2}, (b) 7 mA cm^{-2}, (c) 9 mA cm^{-2}.

PANI film prepared with 7 mA cm^{-2} current density has comparably more fibril nature on surface than that of other PANI samples. It is reported that having fibril form morphology is desirable for electrode materials of redox capacitors, as it may provide a large electrochemical surface area that enables the effective and rapid access of electrolyte [34].

Therefore, compared to other current densities, performance enhancement of PANI films prepared with 7 mA cm^{-2} current density can be attributed to this change in morphological, structural and electrochemical properties.

4. Conclusion

Redox capacitors based on PANI electrodes were fabricated by varying polymerization current density and the effect of the polymerization current density on the performance of the redox capacitors was investigated. Electrochemical impedance spectroscopy showed that redox capacitors have capacitive behavior and low relaxation time which suggests that redox reactions are taking place very quickly. Minimum charge transfer resistance occurs with the redox capacitor fabricated with the electrodes polymerized using a current density of 7 mA cm^{-2}. Cyclic voltammetry studies showed good reversibility of the electrochemical system and 80% of specific charge retention of its initial value was recorded for redox capacitor with 7 mA cm^{-2} polymerization current density. Continuous charge discharge test for 200 cycles also proves that redox capacitor with electrodes

polymerized using 7 mA cm^{-2} current density showed the highest performance with specific discharge capacity of 421.4 F g^{-1}, specific energy density of 8.0 Wh kg^{-1}, specific power density of 935.6 W kg^{-1} and energy efficiency of 85.0%. Morphological studies confirmed the results of the other tests. It can be concluded that higher polymerization current densities enhance the performance of the PANI redox capacitor but there exists a peak value beyond that performances fade with the further increment of the current density.

Acknowledgements

Authors wish to acknowledge the assistance given by National Science Foundation, Sri Lanka under the research grant RG/2014/BS/01, RG/2015/EQ/07 and Wayamba University of Sri Lanka (SRHDC/RP/04/16-17(R2)).

Conflict of interest

All authors declare no conflicts of interest in this paper.

References

1. Zhang X, Lin Z, Chen B, et al. (2014) Solid-state flexible polyaniline/silver cellulose nanofibrils aerogel supercapacitors. *J Power Sources* 246: 283–289.
2. Ryu KS, Kim KM, Park NG, et al. (2002) Symmetric redox supercapacitors with conducting polyaniline electrodes. *J Power Sources* 103: 305–309.
3. Lee J, Lee S (2016) Applications of novel Carbon/AlPO4 hybrid-coated $H_2Ti_{12}O_{25}$ as a high-performance anode for cylindrical hybrid supercapacitors. *ACS Appl Matter Interfaces* 8: 28974–28981.
4. Lee B , Lee S (2017) Application of hybrid supercapacitor using granule $Li_4Ti_5O_{12}$ / activated carbon with variation of current density. *J Power Sources* 343: 545–549.
5. Lee J, Kim H, Baek H, et al. (2016) Improved performance of cylindrical hybrid supercapacitor using activated carbon / niobium doped hydrogen titanate. *J Power Sources* 301: 348–354.
6. Lee S, Kim J, Yoon J (2018) Laser scribed Graphene cathode for next generation of high performance hybrid supercapacitors. *Scientific Reports* 8: 8179–8188.
7. Arslan A, Hür E (2012) Supercapacitor applications of polyaniline and poly(N-methylaniline) coated pencil graphite electrode. *Int J Electrochem Sci* 7: 12558–12572.
8. Kulkarni SB, Patil UM, Shackery I, et al. (2014) High-performance supercapacitor electrode based on a polyaniline nanofibers / 3D graphene framework as an efficient charge transporter. *J Mater Chem A*2: 4989–4998.
9. Liu Q, Nayfeh MH, Yau ST (2010) Supercapacitor electrodes based on polyaniline–silicon nanoparticle composite. *J Power Sources* 195: 3956–3959.
10. Eftekhari A, Li L, Yang Y (2017) Polyaniline super capacitors. *J. Power Sources* 347: 86–107.
11. Patil DS, Pawar SA, Devan RS, et al. (2014) Polyaniline based electrodes for electrochemical supercapacitor: Synergistic effect of silver, activated carbon and polyaniline. *J Electroanal Chem* 724: 21–28.

12. Bhadra J, Al-Thani NJ, Madi NK, et al. (2017) Effects of aniline concentrationson the electrical and mechanical properties of polyaniline polyvinyl alcohol blends. *Arab J Chem* 10: 664–672.
13. Wang G, Hu X, Wong TKS (2001) Effect of deposition current density on the effectiveness of electropolymerized hoe-transport layer in organic electroluminescent device. *Appl Surface Sci* 174: 185–190.
14. Eftekhari A, Jafarkhani P (2014**)** Galvanodynamic synthesis of polyaniline: a flexible method for the deposition of electroactive materials. *J Electroanal Chem* 717–718: 110–118.
15. Jayathilake YMCD, Perera KS, Vidanapathirana KP (2015) Preparation and characterization of a polyacrylonitrile-based gel polymer electrolyte complexed with 1 methyl-3 propyl immidazolium iodide. *J Solid State Electrochem* 19: 2199–2204.
16. Bandaranayake CM, Jayathilake YMCD, Vidanapathirana KP, et al. (2015) Performance of a sodium thiocyanate based gel polymer electrolyte in redox capacitors. *Sabaragamuwa University J* 14: 149–161.
17. Kumar GG, Munichandraiah N (2000**)** A gel polymer electrolyte of magnesium triflate. *Solid State Ionics* 128: 203–210.
18. Prasad KR, Munichandraiah N (2002**)** Potentiodynamically deposited polyaniline on stainless steel inexpensive, high-performance electrodes for electrochemical supercapacitors. *J Electrochem Soc* 149: A1393–A1399.
19. Tey JP, Careem MA, Yarmo MA, et al. (2016) Durian shell-based activated carbon electrode for EDLCs. *Ionics* 22: 1209–1217.
20. Wang W, Guo S, Penchev M, et al. (2013) Three dimensional few layer graphene and carbon nanotube foam architectures for high fidelity supercapacitors. *Nano Energy* 2: 294–303.
21. Harankahawa N, Weerasinghe S, Vidanapathirana K, et al. (2017) Investigation of a pseudo capacitor with polyacrylonitrile based gel polymer electrolyte. *J Electrochem Sci Technol* 8: 107–114.
22. Eftekhari A (2018) The mechanism of ultrafast supercapacitors. *J Mater Chem A* 6: 2866–2877.
23. Prabaharan SRS, Vimala R, Zainal Z (2006**)** Nanostructured mesoporous carbon as electrodes for supercapacitors. *J Power Sources* 161: 730–736.
24. Ramya R, Sivasubramanian R, Sangaranarayanan MV (2013**)** Conducting polymers-based electrochemical supercapacitors—progress and prospects. *Electrochim Acta* 101: 109–129.
25. Bandyopadhya P, Kuila T, Balamurugan J, et al. (2017) Facile synthesis of novel sulfonated polyaniline functionalized graphene using m-aminobenzene sulfonic acid for asymmetric supercapacitor application. *Chem Eng J* 308: 1174–1184.
26. Yu T, Zhu P, Xiong Y, et al. (2016) Synthesis of microspherical polyaniline/graphene composites and their application in supercapacitors. *Electrochim Acta* 222: 12–19.
27. Xu J, Ding J, Zhou X, et al. (2017) Enhanced rate performance of flexible and stretchable linear supercapacitors based on polyaniline @ Au @ carbon nanotube with ultrafast axial electron transport. *J Power Sources* 340: 302–308.
28. Chang W, Wang C, Chen C (2016) Plasma-Induced Polyaniline Grafted on Carbon Nanotube-embedded Carbon Nanofibers for High-Performance Supercapacitors. *Electrochim Acta* 212: 30–140.
29. Molapo KM, Ndangili P, MAjayi RF, et al. (2012) Electronics of Conjugated Polymers (I): Polyaniline. *Int J Electrochem Sci* 7: 11859–11875.

30. Laheäär A, Przygocki P, Abbas Q, et al. (2015) Appropriate methods for evaluating the efficiency and capacitive behavior of different types of supercapacitors. *Electrochem Com* 60: 21–25.
31. Prasad KR, Munichandraiah N (2002) Electrochemical Studies of Polyaniline in a Gel Polymer Electrolyte, High Energy and High Power Characteristics of a Solid-State Redox Supercapacitor. *Electrochem Solid-State Lett* 5: A271–A274.
32. Ryu KS, Kim KM, Park YJ, et al. (2002) Redox supercapacitor using polyaniline doped with Li salt as electrode. *Solid State Ionics* 152–153: 861–866.
33. Du X, Xu Y, Xiong L, et al. (2014) Polyaniline with high crystallinity degree: Synthesis, structure, and electrochemical properties. *J Appl Polym Sci* 131: 6–13.
34. Deshmukh PR, Shinde NM, Patil SV, et al. (2013) Supercapacitive behavior of polyaniline thin films deposited on fluorine doped tin oxide (FTO) substrates by microwave-assisted chemical route. *Chem Eng J* 223: 572–577.

AIMS Press